Title

Multisized Photoannealable Microgels Regulate Cell Spreading, Aggregation, and Macrophage Phenotype through Microporous Void Space

Permalink

https://escholarship.org/uc/item/2b2538w2

Journal

Advanced Healthcare Materials, 12(13)

ISSN

2192-2640

Authors

Lowen, Jeremy M
Bond, Gabriella C
Griffin, Katherine H
et al.

Publication Date

2023-05-01

DOI

10.1002/adhm.202202239

Peer reviewed

Multisized Photoannealable Microgels Regulate Cell Spreading, Aggregation, and Macrophage Phenotype through Microporous Void Space

Jeremy M. Lowen[1,2], **Gabriella C. Bond**[1], **Katherine H. Griffin**[1,3], **Nathan K. Shimamoto**[1], **Victoria L. Thai**[1,2], **J. Kent Leach**[1,2,*]

[1]Department of Orthopaedic Surgery, UC Davis Health, Sacramento, CA 95817

[2]Department of Biomedical Engineering, University of California, Davis, CA, 95616

[3]School of Veterinary Medicine, University of California, Davis, CA 95616

Abstract

Microgels are an emerging platform for *in vitro* models and guiding cell fate due to their inherent porosity and tunability. This work describes a light-based technique for rapidly annealing microgels across a range of diameters. Utilizing 8-arm PEG-vinyl sulfone, we stoichiometrically control the number of arms available for crosslinking, functionalization, and annealing. We fabricate small and large microgels to explore how microgel diameter impacts void space and the role of porosity on cell spreading, cell aggregation, and macrophage polarization. Mesenchymal stromal cells spread rapidly in both formulations, yet the smaller microgels permit a higher cell density. When seeded with macrophages, the smaller microgels promote an M1 phenotype, while larger microgels promote an M2 phenotype. As another application, we leverage the inherent porosity of annealed microgels to induce cell aggregation. Finally, we implant our microgels to examine how different size microgels influence endogenous cell invasion and macrophage polarization. The use of ultraviolet light allows for microgels to be noninvasively injected into a desired mold or wound defect before annealing, and microgels of different properties combined to create a heterogeneous scaffold. This approach is clinically relevant given its tunability and fast annealing time.

Graphical Abstract

Microgels are an emerging platform that have significant advantages over conventional bulk hydrogels including microporosity, modularity, and ability to decouple pore size from stiffness. Differences in microgel size directly correlate with porosity, which in turn influences how cells spread, interact, and ultimately their phenotype. Injectability and an annealing time of 1 minute make microgels a promising therapeutic for the clinic.

*Address for correspondence: J. Kent Leach, Ph.D., Department of Orthopaedic Surgery, UC Davis Health, 4860 Y St., Suite 3800, Sacramento, CA 95817, jkleach@ucdavis.edu.
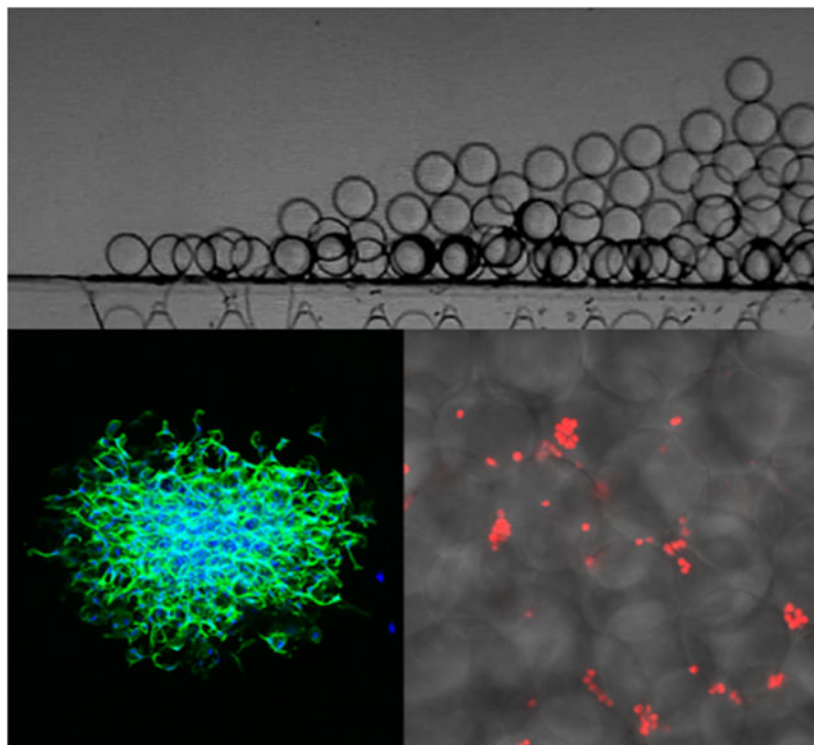
Keywords

Microgels; photoanneal; porosity; macrophage polarization; hydrogel

1. Introduction

Tunable scaffolds that direct cell fate are desirable in many tissue engineering applications such as wound healing, organoid systems, and drug delivery.[1,2] As our understanding of tissue complexity increases, so does the demand for heterogeneous biomaterials.[3] Microgels are an emerging tool that fulfill this role given their modularity, injectability, and range of fabrication techniques.[4-6] Microgels have been harnessed to study cell behavior in response to stiffness, degradability, and biochemical cues.[4,7-9] These granular hydrogels can be synthesized with a variety of polymers including alginate, poly(ethylene) glycol (PEG), and hyaluronic acid.[4,10] Given the array of materials and tunability, microgels can be synthesized to meet a variety of scaffold specifications.

Polymeric scaffolds are frequently bulk hydrogels possessing a nanoporous mesh size that impedes cell infiltration, migration, and hinders biological activity.[11] As a result, the inclusion of a hydrolytic or matrix metalloproteinase (MMP)-sensitive crosslinker is often used to enable cells to degrade and remodel their surrounding environment.[12] Cells will secrete MMPs in response to environmental stimuli, such as macrophages that secrete MMP-9 in response to infection.[13]

Unlike bulk hydrogels, microparticle-based scaffolds possess tunable void space which inherently exists between the particles. Such void space permits cells to migrate and proliferate readily without first remodeling their surrounding environment. For example, human dermal fibroblasts proliferated two-fold more in a microgel scaffold compared to a bulk hydrogel scaffold.[14] However, many techniques of microgel assembly have several primary drawbacks. The use of enzymatic catalysis to anneal microgels can take up to 90 minutes.[10] Enzymatic catalysis may also require the use of costly reagents such as Factor XIII.[7,14] Furthermore, there is a limited understanding for how microgel diameter affects void space and cell behavior. While the effects of pore size on cell penetration and proliferation have been well studied in bulk hydrogels, it has yet to be thoroughly investigated in a microgel platform.[15,16]

Many microgel platforms rely on chemical assembly methods such as enzymatic catalysis[7,14,17] or click chemistry[18,19]. While UV photoannealing has been utilized previously for microgels,[20] previous studies with PEG-vinyl sulfone microgels show a storage modulus reaching a peak of 578 Pa.[6] Herein, we demonstrate an ultraviolet (UV) method of annealing microgels that enables broad control over substrate mechanical properties. This method is effective to anneal microgels with a range of diameters and requires as little as one minute for annealing. The combination of annealing solution, photoinitiator, and stoichiometric control permit our scaffolds to reach a storage modulus of over 2 kPa. Our annealing method adds to the list of tools available in the rapidly growing microgel field, and our cell studies offer insight to how different cell types interact with our unique microgel sizes and chemistry.

We employ the ability to readily alter porosity in photoanneable microgel scaffolds to influence macrophage polarization, alter cell spreading and aggregation, and influence cell function. We generate microgels with compressive moduli ranging from ~ 10-80 kPa, which demonstrates their ability to match a range of tissue stiffnesses.[21] We further show the compressive modulus and bioactivity of the microgels remain constant after cryopreservation at −20°C, which facilitates high-throughput production, storage, off-the-shelf availability, and expands their potential for clinical translation. Finally, we interrogate how microgel diameter influences cell invasion upon implantation. The ease of loading cells, cryopreservability, and short annealing time make this a promising platform for translation to the clinic.

2.   Results and Discussion

2.1   Synthesis and annealing of microgels

Microgels were synthesized using a previously established high-throughput microfluidic device capable of producing up to 30 mL h^{-1} (Figure S1, Supporting Information). [14] We fabricated devices with different channel heights to produce microgels of different diameters. The use of an 8-arm PEG-vinyl sulfone (PEG-VS) allows us to fine tune the number of arms used for crosslinking while leaving arms available for biofunctionalization with peptides. To facilitate microgel annealing, we crosslinked a fraction of the arms and kept the remaining free arms available for photoannealing (Figure 1A). We stoichiometrically controlled the number of free arms by altering the ratio of 8-arm

PEG-VS to the crosslinker PEG-dithiol (PEG-DT). By using the vinyl sulfone moiety for both microgel crosslinking and annealing, we avoid the use of additional complex or costly reagents required for enzymatic catalysis or host-guest interactions.[22,23]

To anneal the microgels, we added our annealing solution of PEG-DT in HEPES with photoinitiator (Figure 1B). The microgels were then spun down and supernatant removed. For larger microgels, a higher centripetal force is required to effectively jam the microgels due to the increased void space between them. The aggregated microgels may be mixed with cells or other additives, as the microgels exhibit shear thinning behavior and can easily be manipulated. The microgel slurry was plated and exposed to UV light to finish the annealing process. To determine necessary time for annealing, we measured the storage modulus of microgel slurries during UV exposure (Figure 1C). We found UV exposure at 20 mW cm^{-2} for 1 minute significantly increased storage modulus, while 2 minutes resulted in a stronger annealing response. The increase in storage modulus in the control group without UV light can be attributed to slight annealing of the microgels through Michael Addition. This could be modulated by changing the pH of the annealing solution. Our approach is advantageous compared to other methods that may require hours for assembly.[22,24] Furthermore, the capacity to anneal microgels at room temperature with only a UV light source increases clinical accessibility. This strategy is amenable to the use of other photoinitiators sensitive to different wavelengths such as those found in the visible light spectrum (*e.g.*, eosin Y).[17]

We created microgels with 50, 60, and 70% of the arms crosslinked to determine how many of the VS groups to leave for annealing. We tested the compressive moduli of scaffolds made from these microgels to observe how strongly they were annealed. We also tested the addition of N-vinyl-2-pyrrolidone (NVP), which has been reported to increase gelation of PEG-VS by increasing the diffusion of free radicals.[25,26] We found the addition of PEG-DT necessary to promote annealing, while the inclusion of NVP increased the annealing strength across all groups (Figure 1D). Microgels with 60% of the arms crosslinked before annealing resulted in the highest compressive modulus. We hypothesize this is due to crosslinking a sufficient fraction of arms to increase the compressive moduli of a microgel while leaving enough arms free to anneal neighboring microgels. Based on these results, the remainder of our studies utilized microgels with 60% of the PEG-VS arms crosslinked. We also tested several concentrations of PEG-DT in our annealing solution, with a 4.8 mM concentration theoretically being the maximum concentration needed to fully crosslink the remaining PEG-VS arms in 3% w/v PEG-VS microgels (Figure 1E). While 2 mM resulted in a large portion of the microgels dissociating from the scaffold, 5 mM and 10 mM PEG-DT resulted in similar amounts of dissociation, indicating the vinyl sulfone groups were fully saturated with 5 mM. This indicates the annealing reaction is efficient enough to not require excess PEG-DT beyond that needed to crosslink the remaining arms. As a result, we utilized solutions of PEG-DT with a concentration matching the concentration of free arms for annealing in further experiments.

Finally, we verified that we could create microgel scaffolds that were of clinically relevant dimensions (Figure S2, Supporting Information). We fabricated microgel scaffolds that were up to 1 cm in thickness, confirming the microgels do not significantly attenuate UV light in large scaffolds. Furthermore, the 1 cm thick photoannealed microgel scaffold withstood

cyclically applied compression, demonstrating the strength of the annealed scaffold (Video S1, Supporting Information). This approach was designed to minimize the steps needed for scaffold formation. By stoichiometrically controlling the number of arms used for crosslinking and annealing, we minimize the number of reagents needed to form an annealed microgel scaffold.

2.2 Mechanical properties and assessing potential for microgel cryopreservation

The design and application of microgels requires an accurate understanding of their mechanical properties. Scaffolds are commonly engineered to match the mechanical moduli of the target tissue.[27] There is a lack of research on how the microscale properties of a material compare to the macroscopic properties of its bulk counterpart. We utilized a MicroTester to test the compressive modulus of individual microgels (Figure 2A). This device allowed us to measure the mechanical modulus of individual microgels by measuring force and displacement of the microgel (Video S2, Supporting Information).

We compared the mechanical properties of our individual microgels to conventional PEG-VS bulk gels (Figure 2B). As expected, all groups followed a similar trend of increased compressive modulus with increased concentration of PEG-VS. We generated microgels with stiffnesses ranging from ~10 – 82 kPa with macromer concentrations of 3% and 12%, respectively. A larger range of mechanical properties could be generated by lowering or raising the macromer concentration. The moduli of the individual microgels were higher than their respective bulk gels in the 9% and 12% conditions. This could be due to the difference in testing methods, as microgels were tested on a MicroTester and the bulk gels were tested on an Instron. Alternatively, this could be due to individual microgels being more homogeneous than their bulk counter parts, which often may not be uniformly smooth or crosslinked. The slight heterogeneity of bulk gels may yield a softer modulus. We also compared the moduli of microgels made from 10 kDa versus 20 kDa PEG-VS. The 10 kDa microgels trended toward a higher modulus due to the monomers having shorter arms which results in closer packing (Figure 2C). We selected the 10 kDa PEG-VS for the remainder of our studies due to the capacity to fabricate microgels with a larger range of stiffness.

The ability of the microgels to be cryopreserved is important for long-term storage, production in a high-throughput manner, and for clinical application. Recently, microgels have been cryopreserved in the pursuit of reproducible particle size after rehydration.[28] We performed mechanical testing on 6% PEG-VS microgels frozen at −20°C for up to a month and observed no change in mechanical properties when tested upon thawing (Figure 2D). We also assessed the ability of RGD-functionalized microgels to remain bioactive after cryostorage. Peptides can be utilized to influence cell behavior such as attachment or differentiation.[29] We verified that we could functionalize our microgels using fluorescent peptides. The fluorescent peptide was clearly present on the microgels both upon synthesis and after 3 days (Figure 2E). These findings confirmed that washing and collection steps did not impede peptide attachment. We observed comparable cell spreading by human mesenchymal stromal cells (MSCs) in both frozen and freshly made microgels compared to unmodified microgels (Figure 2F). Interestingly, the cells in microgels without peptides formed cellular aggregates, most likely due to the lack of adhesive sites on the microgels and

the cell-cell adhesion that occurred. Fresh and frozen microgels supported similar levels of cellular metabolic activity (Figure 2G).

By measuring the mechanical properties of the microgels and demonstrating their ability to be cryopreserved, we further illustrate their potential utility in the clinic. The large range of stiffnesses and ability to impart bioactivity via peptide incorporation enable these microgels to be tailored for a variety of applications. The microgels demonstrate their ability to maintain a constant compressive modulus and peptide function after cryopreservation, opening the door for on-demand use in the clinic.

2.3 Modeling of void space in annealed microgels

The porosity of our microgel scaffolds is a strong predictor for how cells may migrate, aggregate, and differentiate within our constructs. Smaller diameter microgels will have less void space between them, and therefore, cells will be increasingly monodispersed with less room to spread. Conversely, larger diameter microgels will possess increased void space between them so cells will be able to more easily migrate and aggregate. Similarly, more polydisperse microgels will exhibit larger void space due to the microgels being unable to pack together in an optimal manner.

To simulate microgel packing, we used MATLAB to identify and measure the diameters of batches of large and small microgels (Figure 3A). Large microgels had an average diameter of 146.1 ± 2.7 μm, while small microgels had an average diameter of 47.9 ± 4.1 μm (Figure 3B). The slightly larger standard deviation in the smaller microgels can be attributed to the increased surface area-to-volume ratio requiring more surfactant. We then imported the measured diameters into a custom MATLAB script based on established code[30] which will close pack the microgels and minimize the sum of distances between them (Figure 3C). The microgels will converge to hexagonal close packing (HCP) with greater monodispersity.

We used ImageJ to calculate the area of the void space between the microgels (Figure 3D). For the more monodisperse large microgels, much of the void space area is triangular due to convergence to HCP, while some larger theoretical areas are observable between the more polydisperse microgels. We used microscopy to measure the void space area in annealed scaffolds and found that the actual average void space between microgels was not significantly different from our predicted area (Figure 3E). Minor variance between the two could be attributed to the microgels slightly compressing or packing imperfectly. While actual diameters were used in the modeling, a list of theoretical diameters could be inputted to predict what other void spaces may result.

The ability to model void space is beneficial for many cell-based projects that vary greatly in the scale of biologics used. There are significant differences between cell types such as red blood cells and adipocytes which can range from 7.5 μm to over 100 μm in diameter, respectively.[31,32] Aggregates of cells such as MSC spheroids can reach up to 600 μm without a hypoxic core.[33] It is also useful for the incorporation of other additives such as drug-loaded nanoparticles.[34] Overall, modeling is a powerful tool that can be utilized to fabricate microgels for a specific porosity to influence cell phenotype.

2.4 Evaluation of annealed microgels to promote formation of cell aggregates

Multicellular spheroids can act as building blocks that capture complex aspects of *in vivo* environments and represent improved model systems to study development and disease. Spheroids exhibit increased viability along with enhanced proangiogenic, anti-inflammatory, and tissue-forming potential.[35] Thus, the development of a platform that can promote the formation of cellular aggregates would be useful for many tissue engineering applications. To further investigate the impact of microgel size on cellular aggregate formation, we seeded monodisperse MSCs in small and large microgel scaffolds lacking adhesive motifs to encourage cell-cell adhesion and promote aggregate formation. We observed spheroid formation over the first 48 hours, which is a typical timeframe for spheroid formation using other methods such as hanging drop[36] or formation in non-adhesive well plates.[37,38]

Aggregate formation was visible in large diameter microgel scaffolds after 12 hours, with monodisperse cells still present throughout the scaffold. The average aggregate size was consistent over 48 hours. MSCs in small diameter microgels formed smaller aggregates after 12 hours with many cells remaining monodisperse (Figure 4A). We observed a trend towards a smaller aggregate diameter over 48 hours, which may be due to compaction of the aggregates.[35] Quantification of average aggregate size over time illustrates how the void space in large microgel scaffolds promotes increased aggregate size compared to small microgel scaffolds (Figure 4B). The average aggregate diameters at 48 hours in the large and small microgel scaffolds were ~32.0 μm and 14.8 μm, respectively, which strongly correlates with the observed void space areas in Figure 3E.

Confocal microscopy of large diameter microgel scaffolds at 48 hours allowed us to clearly visualize aggregates through the scaffold (Figure 4C). While some cells remained monodisperse, the majority were contained in aggregates. We observed minimal cell spreading, possibly due to the deposition of extracellular matrix (ECM) by the MSCs. Furthermore, we were able to dissociate the microgels and retrieve viable cellular aggregates (Figure 4D). For this application, we weakly annealed the microgels by avoiding NVP in our annealing solution, which permitted dissociation by simple pipetting. This demonstrates the potential for microgels to be used as a spheroid formation platform, where spheroids can be formed and collected for use in another medium. However, the aggregates formed in this platform are significantly smaller compared to aggregates achievable *via* other methods such as hanging drop, which has resulted in aggregates over 1000 μm in diameter.[36] While this platform may not be able to generate aggregates as large as established methods, it is feasible that larger microgels could yield larger aggregate formation as needed. A scaffold which promotes spheroid formation may eliminate the need to form spheroids *a priori*, which commonly requires a minimum of 48 hours.[37] Given the correlation between our model of void space and aggregate size, it would be possible to design specific size microgels for formation of a desired spheroid size.

2.5 Effects of microgel diameter on cell proliferation and spreading

The void space between microgels allows for rapid cell infiltration and proliferation without cells needing to remodel the surrounding environment, as is required in bulk hydrogels.[8] To assess how void space influences cell spreading, we seeded spheroids in scaffolds composed

of large and small microgels. By seeding the microgels with spheroids, we can examine migration distance and density which is not possible if the cells were distributed throughout as monodisperse cells. Microgels increase MSC retention and proliferation compared to traditional nanoporous hydrogels.[40] However, spheroid growth in our specific microgel sizes has not been reported. We hypothesized the increased surface area present in small microgel scaffolds would promote faster cell migration from the spheroid into the scaffold.

We seeded 15,000 cell spheroids composed of MSCs and endothelial cells at a 2:1 ratio in our microgel scaffolds, as we previously demonstrated this spheroid composition forms robust cellular networks.[41] Microgels were modified with RGD to promote cell adhesion and migration. We assessed network formation and migration distance on Day 1 and Day 7 *via* confocal microscopy and stained cells with phalloidin and DAPI to visualize the actin cytoskeleton and nuclei, respectively (Figure 5A).

Both large and small microgels promoted rapid migration of cells into the scaffold. The leading edge of cell migration was comparable for both microgel sizes on Days 1 and 7 (Figure 5B). The greater porosity within large microgel scaffolds did not significantly hinder cell migration. However, the smaller diameter microgel scaffold resulted in a higher cell density on Days 1 and 7 (Figure 5C). This can be attributed to the higher surface area-to-volume ratio of the smaller microgels that provide more attachment sites for cell spreading. Both scaffolds promoted similar levels of metabolic activity when normalized to DNA, indicating both formulations promote high viability (Figure 5D).

The rapid migration of cells in both conditions highlights the advantage of inherent porosity in microgel scaffolds. The measurable migration on Day 1 reflects the cells ability to immediately migrate without first remodeling the surrounding environment. While void space size is significantly smaller in small microgel scaffolds compared to large microgel scaffolds, it was sufficient to permit cell movement. Future work could utilize different size microgels to regulate the density of cell infiltration and spreading.

2.6   Effects of microgel size on macrophage polarization

Solid biomaterial implants often induce a foreign body response, regulated by macrophages, that is characterized by poor vascularization and fibrosis.[42] Ideally, a biomaterial will promote a pro-regenerative response characterized by cell infiltration and material integration.[43] Microgels can promote a pro-regenerative M2 phenotype compared to clinical controls such as Oasis Wound Matrix decellularized ECM.[44] While the influence of macrophage polarization within a single microgel scaffold has been reported,[45] the impact of altering microgel size and void space on macrophage polarization has not been described.

We seeded IC-21 macrophages in 4.5% PEG-VS large and small microgel scaffolds modified with 1 mM RGD to enable attachment. We also seeded macrophages polarized toward an M1 phenotype to assess how macrophages predisposed toward an inflammatory phenotype respond to differences in void space. We chose this medium stiffness formulation to minimize the effect of substrate stiffness on macrophage polarization.[46,47] Macrophages were collected after 6 days in culture for assessment of polarization *via* flow cytometry. We

utilized our "weak" annealing formulation lacking NVP described in section 2.4 to facilitate macrophage recovery from the gels. A subset of macrophages was stained with CellTrace to permit visualization with fluorescent microscopy and observe their interaction with the microgel scaffolds.

Confocal microscopy of the macrophages revealed that in small microgel scaffolds, macrophages were often sandwiched between individual microgels, with several exhibiting an elongated morphology. Conversely, macrophages easily fit in the void spaces of large microgel scaffolds and generally maintain a rounded morphology (Figure 6A). In some cases, clusters of macrophages can be seen that were not visible in the small microgel scaffold.

Flow cytometry revealed that both microgels supported high cell viability (Figure 6B,E). Macrophages with an M1 phenotype (F4/80+CD86+iNOS+ populations) were more prevalent in small microgel scaffolds with both naïve and polarized macrophages (Figure 6C,F). Macrophages with an M2 phenotype (F4/80+CD206+ARG1+ populations) accounted for significantly more of the macrophages in the large microgel scaffold in both macrophage conditions (Figure 6D,G). These observations agree with earlier work wherein minimizing macrophage adhesion to implants upregulates the M2 phenotype.[42,44,48] We also show similar trends exist between naïve and M1 polarized macrophages. This is relevant to wound or surgical sites where M1 macrophages are typically associated.[49] The increased void space between large microgels limits the amount of contact macrophages have with the scaffold, often with macrophages contacting only one microgel. Conversely, in the small microgel scaffold, macrophages often are contacting multiple microgels at once and are stimulated from all sides. By increasing the porosity, it may be possible to reduce the foreign body response (FBR) to a material and increase the presence of pro-regenerative M2 macrophages as previously reported with other platforms.[50] Microgels are a promising candidate for porous biomaterials given the tunable void space that exists between them. While the porosity in the small microgel scaffold was large enough to promote rapid and dense spreading as demonstrated in section 2.5, it may be so small as to promote unintended effects such as a pro-inflammatory response from macrophages. Therefore, when picking a microgel size, it is important to consider the resultant porosity between them.

2.7   *Microgel scaffolds permit endogenous cell infiltration* in vivo

Finally, we interrogated how cellular infiltration and macrophage polarization *in vivo* may be influenced in scaffolds formed from different sized microgels. We implanted small and large microgel scaffolds in C57BL/6 mice for 2 weeks to assess endogenous cell migration (Figure 7A). We used PDMS molds to prevent infiltration from one side of the scaffold to accurately assess migration from the other side (Figure 7B). Implants were harvested after 2 weeks for histological processing.

Hematoxylin and eosin (H&E) staining revealed that cells tended to migrate further in the large microgel scaffolds (Figure 7C). Where cells did infiltrate, they surround both sizes of microgels, indicating the porosity in both scaffolds was sufficient for migration. The reduced migration depth in the smaller microgel scaffolds could be a result of the smaller porosity hindering migration or the increased surface area resulting in cells spreading out more

densely and impeding invasion. Increased extracellular matrix deposition, evidenced by Masson's trichrome staining, corroborated the increased migration seen in the large microgel scaffolds (Figure 7C). Larger aggregates of cells are present between the larger microgels. Notably, collagen is present primarily around the surface of the implants but is scarce in between the microgels themselves. While this indicates a FBR to the PDMS mold in which the microgel scaffolds were housed, it appears the FBR to the microgels themselves was minimized. Immunohistochemistry revealed the presence of both M1 (iNOS+) and M2 (CD206+) macrophages (Figure 7D). While we did not detect a significant difference in the presence of M2 macrophages, we observed significantly fewer M1 macrophages in the large microgel scaffold (Figure 7E). The reduction in M1 macrophages as a function of microgel diameter *in vivo* agrees with our *in vitro* findings and suggests that increased scaffold porosity could reduce a pro-inflammatory response to implanted materials.

In vivo implantation resulted in robust endogenous cell spreading and infiltration in our microgel scaffolds. The increased surface area of the smaller microgels resulted in denser spreading near the surface of the scaffold but less migration into the scaffold. Conversely, endogenous cells consistently migrated the depth of the larger microgel scaffolds but were more spread out. This study demonstrates microgels are a promising biomaterial to promote rapid cell infiltration and biomaterial integration. Furthermore, these data further illustrate the importance of pore size and its direct effect on cell density and spreading.

3. Conclusion

Microgels have immense potential in tissue engineering and regeneration given their tailorability, clinical accessibility, and inherent porosity which can be decoupled from stiffness. This method has the advantage of a strong annealing strength, short annealing time, inexpensive reagents, and the ability to anneal at room temperature. The microgels exhibit a large range of stiffnesses and can be frozen without degradation or loss of bioactivity of adhered peptides. We modeled and predicted the differences in void space that emerge due to microgel diameter. We demonstrated how the void space in the microgels can be used as a platform for spheroid formation. Furthermore, we established that while both large and small microgel scaffolds promote rapid cell spreading, the smaller microgels provide more surface area and increase cell density. Upon seeding macrophages in different size microgel scaffolds, we observed increased M2 polarization in the larger microgel scaffold. Finally, we observed robust cell invasion and a limited foreign body response when scaffolds were implanted *in vivo*. Large microgel scaffolds had fewer M1 polarized macrophages compared to small microgel scaffolds *in vivo*, corroborating our *in vitro* findings.

This work contributes to the growing body of work on microgels to guide cell behavior. Our approach to rapidly anneal PEG-VS microgels, coupled with their stability upon cryostorage, makes them even more accessible in the clinic or for preclinical studies. Furthermore, we show how our specific microgel sizes of ~48 μm and 146 μm facilitate cell spreading, aggregate formation, and macrophage polarization. As the body of evidence grows, we will gain an increased appreciation for how microgel diameter influences cell behavior. The many variables contributing to microgel scaffolds such as

polymer composition, crosslinker, stiffness, diameter, packing density, and annealing enable tremendous tunability and expand the possible type and techniques to synthesize microgel formulations. This work expands upon the possible combinations and offers insight into how this specific annealing method and microgel formulation could be utilized for research on the bench and in the clinic.

This work demonstrates not only the advantages of microgel scaffolds as an emerging biomaterial, but the importance of designing a biomaterial with the appropriate porosity. Differences in microgel size directly correlate with porosity, which in turn influences how cells spread, interact, and ultimately their phenotype. Microgels are a promising alternative to solid implants or nanoporous bulk hydrogels. They can be delivered in a less invasive manner compared to bulk scaffolds or autologous implants and enable increased porosity compared to conventional bulk hydrogels. The increased cell infiltration and material integration made possible with microgel scaffolds may reduce the foreign body response induced by implants and create an increased pro-regenerative response. Future work can utilize combinations of specifically tailored microgels to target complex tissue repair.

4. Experimental section

Device fabrication:

Microfluidic master molds were created on silicon wafers (University Wafer) for devices first described in Rutte et al.[14] We used a two-layer photolithography process with SU-8 10 and SU-8 100 (Kayaku Advanced Materials) to create channels heights to produce microgels of different diameters. The layers were aligned utilizing a EVG 620-mask aligner, and we used a Bruker Dektak XT to verify the heights of our device channels. A nozzle channel height of 12 μm and 38 μm created droplets of ~48 μm and 146 μm, respectively. We then poured polydimethylsiloxane (PDMS) (Ellsworth Adhesives, Sylgard 184) over our silicon master molds with the base and crosslinker mixed at a 10:1 mass ratio. The PDMS mixture was desiccated and cured at 65°C for at least 1 hr and cut out. PDMS devices and glass slides were plasma cleaned and bonded together followed by a bake of 125°C on a hotplate for 1 hr. The microgel devices were then treated with Aquapel and Novec 7500 Oil (3M) to render the devices hydrophobic and fluorophilic, respectively.

Microgel fabrication:

The microgel device contains a continuous oil phase and a dispersed aqueous phase. For large microgels, the oil phase consisted of Novec 7500 Oil and 0.75 wt% Picosurf (Sphere Fluidics). Picosurf concentration was increased to 2 wt% for the small microgels. The aqueous phase consisted of 8-arm PEG-VS (JenKem) in 0.15 M triethanolamine (TEOA, pH 5.1, Sigma) buffer and 3.5 kDa PEG-DT (JenKem). The solutions were injected into the microfluidic device using syringe pumps (NE-1000 and KD Scientific), with the continuous phase set at twice the flow rate of the dispersed phase. We utilized flow rates of 60/30 μL min^{-1} for the large microgels and 30/15 μL min^{-1} for the small microgels. After exiting the device, microgels were combined with a solution of 1% v/v triethylamine (TEA, Sigma) in Novec 7500 Oil using a Y-junction (IDEX Health and Science) and left at room temperature overnight to ensure complete crosslinking.

Microgel cleaning:

Excess oil was first removed by pipetting. The emulsion was broken by adding a solution of 20 wt% 1H,1H,2H,2H-Perfluoro-1-octanol (Sigma) in Novec 7500 Oil approximately equal to the volume of remaining microgels. Microgels were swelled and dispersed by adding HEPES buffer (25 mM, pH 7.4). The remaining oil was removed by washing in hexane 3x. For cell experiments, the microgels were then sterilized by washing 3x with 70% isopropyl alcohol. Finally, the microgels were washed with sterile HEPES buffer 3x where they were kept until use.

Microgel annealing:

Microgels were first pelleted and then resuspended in 5mM PEG-DT in HEPES containing 0.4% VA-086 photoinitiator (FUJIFILM) equal to the volume of microgels. After incubating for 1 min, the microgels were spun down for 3 min at 3000xg for the small microgels and 15,000xg for the large microgels. The supernatant was then removed and microgels plated in the desired mold utilizing a positive displacement pipette (Gilson). The microgel slurry was then exposed to UV light (20 mW cm^{-2}, 320-500 nm, Omnicure S2000) for 2 min to form annealed scaffolds.

Annealing optimization studies:

Microgels of 6% PEG-VS were created such that 50, 60, and 70% of the PEG-VS arms were crosslinked with PEG-DT. Microgels with fewer crosslinked arms did not maintain their shape, while microgels with more crosslinked arms did not anneal sufficiently. Microgels were then soaked in a solution containing 0.4% photoinitiator in HEPES, HEPES + 10 mM PEG-DT, HEPES + 0.1 v/v% NVP (Sigma), or HEPES + 10 mM PEG-DT + 0.1 v/v% NVP. Microgel scaffolds were formed as detailed previously and mechanical testing was performed as described below.

Formation of large microgel constructs:

We first poured PDMS into a petri dish until it was 1 cm tall. After curing, we created an 8 mm x 1 cm cylindrical mold in the PDMS using an 8 mm biopsy punch. Microgels were then pipetted and annealed as described above.

Bulk hydrogel fabrication:

Separate solutions of PEG-VS dissolved in diH$_2$O (pH = 5.5) and PEG-DT dissolved in diH$_2$O (pH = 8.5) were prepared at twice the concentration of their microgel counterparts. 50 μL of each solution was pipetted into 8 mm x 1.5 mm cylindrical molds and mixed by pipetting up and down. After 10 minutes the gels were removed, put into a solution of HEPES (25 mM, pH = 7.4), and allowed to swell overnight.

Mechanical characterization:

Bulk hydrogel scaffolds were measured using an Instron 3345 Compressive Testing System (Norwood, MA). Hydrogels were loaded between two flat platens and compressed at a rate of 0.05 mm/s. Moduli were calculated from the slope of stress versus strain plots limited to the linear first 10% of strain.[51] Microgels were examined using a MicroTester (CellScale,

Waterloo, ON). Individual microgels were loaded onto an anvil in a water bath filled with PBS. The microgels were then compressed half their diameter by a stainless-steel platen attached to a tungsten rod over 30 s. Displacement and force was tracked *via* MicroTester software. The linear region of the of compressive modulus vs nominal strain graph was recorded as the calculated modulus.[52] Storage modulus of microgel scaffolds over time was measured using a Discovery HR2 Rheometer (TA Instruments, New Castle, DE) with a stainless steel, cross hatched, 8 mm plate geometry. For our experimental group, the scaffolds were exposed to UV light after 30 s, while it remained off the entire time for our control group. A custom oscillatory time sweep (1% strain, 1rad/s angular frequency) was performed using an initial 0.03N normal force.

Verification of peptide conjugation:

We added 2 mM fluorescently tagged HAVDI (FITC-HAVDIGGGC, WatsonBio) to our microgels which crosslinked to some of the PEG-VS arms during synthesis *via* Michael Addition. Microgels were immediately imaged upon synthesis as well as 3 days post-synthesis and washing.

Cell culture:

Human endothelial colony forming cells (ECFCs) were isolated and derived from human cord blood obtained through the UC Davis Cord Blood Collection Program (UCBCP). ECFCs were expanded in EGM-2 supplemented media (PromoCell, Heidelberg, Germany) with gentamicin (50 μg mL^{-1}; ThermoFisher, Waltham, MA) and amphotericin B (50 ng mL^{-1}; ThermoFisher) under standard culture conditions (37°C, 5% CO_2, 21% O_2) until use at passages 7-8. Media changes were performed every 2 days. Human bone marrow-derived MSCs (RoosterBio) from a single donor (21-year-old male) were expanded in growth medium (GM) consisting of minimum essential alpha medium (α-MEM; Invitrogen) supplemented with 10% fetal bovine serum (FBS; Genesee) and 1% penicillin/streptomycin (Gemini Bio-Products, Sacramento, CA). MSCs were cultured under standard conditions until use at passage 4. Media changes were performed every 2–3 days.

Influence of cryostorage on microgels:

We fabricated 6% PEG-VS large diameter microgels with 1 mM RGD (Ac-RGDSPGERCG-NH$_2$, Genscript). Microgels were frozen for up to one month at −20°C, with batches being removed, thawed, and analyzed at designated time points. Mechanical testing was performed on the MicroTester as described above. After 1 week in storage, microgels were seeded with human MSCs (RoosterBio) at 5 million cells mL^{-1} and compared to fresh microgels when maintained in complete medium for 48 hr. Metabolic activity of seeded MSCs was determined by alamarBlue assay (Thermo Fisher). The cell actin cytoskeleton was stained with Alexa Fluor 488 Phalloidin solution (Thermo Fisher; 1:400 in PBS), and cell nuclei were stained with DAPI (Thermo Fisher; 1:500 in PBS). Z-stacks were taken on a confocal microscope (Leica Stellaris 5), and max projections used to illustrate cell morphology through the scaffolds.

Modeling of void space:

A custom MATLAB code was created to measure microgel diameters and model annealing. Annealed scaffolds were imaged *via* microscopy and ImageJ was used to measure the void space area between microgels.

Formation of cell aggregates within scaffolds:

Small and large microgel scaffolds composed of 6% PEG-VS were seeded with MSCs at 5 million cells mL^{-1}. Images were acquired at 12, 24, and 48 hr with brightfield microscopy (Nikon Eclipse TE2000U). Aggregates from large microgels were collected by pipetting the scaffolds up and down, followed by pipetting the solution through a 100 μm sieve. Aggregates were washed with PBS, stained with a live/dead assay per the manufacturer's protocol (Thermo Fisher), and fluorescent images taken using the Nikon Eclipse TE2000U. For confocal microscopy images, cells were stained and imaged with DAPI and phalloidin as described above. Aggregate size was measured in ImageJ using the line and measurement tools.

Assessment of spreading in scaffolds from co-culture spheroids:

Heterotypic co-culture spheroids were formed with ECFCs and MSCs at a ratio of 1-to-2 using a forced aggregation method.[37,38] Briefly, desired concentrations of ECFCs and MSCs were pipetted into 1.5% agarose molds in well plates, and the plates were centrifuged at 500xg for 8 min. Plates were maintained in static standard culture conditions (37°C, 5% CO_2, 21% O_2) for 48 hr to enable spheroid formation in 3:1 EGM-2:α-MEM. Each microwell in the agarose molds contained 15,000 cells. 4.5% PEG-VS microgels with 1 mM RGD were used for the large and small microgel scaffolds. Microgels were annealed as described above, with the microgel slurry being mixed with heterotypic spheroids before being plated in a 6 mm x 1.5 mm cylindrical silicon mold and exposed to UV light. Scaffolds were collected for analysis on Day 1 and Day 3, with media changed every other day using the 3:1 mixture of EGM-2:α-MEM. For confocal microscopy images, cells were stained and imaged with DAPI and phalloidin as described above. Metabolic activity of spheroids was determined by alamarBlue assay (Thermo Fisher). DNA content was quantified using the PicoGreen Quanit-iT Assay Kit (Invitrogen). Migration distance and cell density were quantified in ImageJ using the Li threshold.

Assessment of macrophage polarization as a function of microgel diameter:

IC-21 murine macrophages (ATCC) were seeded at 4 million cells mL^{-1} in small or large microgel scaffolds. To polarize macrophages toward an M1 phenotype, lipopolysaccharide (LPS, 0.3 ng mL^{-1}, Thermo Fisher) was added 48 hr before seeding and refreshed with basal media after 24 hr. Microgels were formed from 4.5% PEG-VS with 1 mM RGD prepolymer solution. Microgel and macrophage slurries were pipetted into 8 mm x 5 mm cylindrical molds before exposure to UV light. The gels were maintained in RPMI 1640 (ATCC) supplemented with 10% FBS. After 24 hr, gels were moved to a new plate with fresh media and maintained in culture for 6 days with media changes every day. For confocal microscopy, 8 mm x 1.5 mm scaffolds were prepared and imaged on the Leica Stellaris 5. Cells were recovered from annealed patties *via* digestion at 37°C with trypsin for 5 min and

gentle mixing, followed by dilution with basal media. Solutions were filtered through a 30 μm sieve to create a single cell suspension, and macrophage polarization was characterized using flow cytometry (Attune NxT, Life Tech).

Flow cytometry:

Following Fcγ receptor blocking (1:40, TruStain FcX, BioLegend), cells were stained with antibodies against F4/80 (1:50, eBioscience #MF48021), CD86 (1:160, eBioscience #47-0862-82) and CD206 (1:40, eBioscience #48-2061-82). Cellular viability was evaluated with fixable Zombie Aqua (1:250, Life Tech). Cells were then fixed with 2% PFA, permeabilized with 0.1% Triton-X, and stained for intracellular markers, iNOS (1:500, eBioscience #12-5920-82) and Arginase-1 (1:500, eBioscience #53-3697-82), overnight at 4°C with gentle agitation. Macrophages with an M1 phenotype were characterized by F4/80+CD86+iNOS+ populations and M2 phenotypes by F4/80+CD206+ARG1+ populations. The frequency of each type of macrophage was quantified per microgel size. Polarization controls (data not shown) consisted of IC-21s seeded on TC wells in monolayer treated with basal media (M0), 200 ng/mL LPS (M1), and 20 ng/mL IL-4 (M2) for 24 hr. Cells were lifted with trypsin and gentle agitation. Cells were filtered and stained as described.

Subfascial Implants:

Before implantation, 4.5% PEG-VS microgels with 1 mM RGD were loaded and annealed in PDMS molds. Treatment of experimental animals was in accordance with UC Davis animal care guidelines (IACUC protocol #22577; Animal Welfare Assurance #D16-00272) and all National Institutes of Health animal handling procedures. Male twelve-week-old C57BL/6 mice (Jackson Laboratories, West Sacramento, CA) were anesthetized and maintained under a 2% isoflurane/O_2 mixture delivered through a nose cone. Each animal received four subfascial implants: small microgels (upper and lower left) and large microgels (upper and lower right). Following a dorsal midline incision, fascia was incised, and blunt dissection was performed between the fascia and muscle belly. Annealed microgels in PDMS molds were placed face-down on the muscle and sutured in place with 4-0 Monocryl sutures (Ethicon, Cornelia, GA). Animals were euthanized after 2 weeks, and gels were collected, removed from PDMS, and fixed in 4% PFA overnight at 4°C. Samples were then washed twice in PBS, paraffin-embedded, and sectioned at 7 μm. Sections were stained with hematoxylin (Thermo) and eosin (Ricca) (H&E) or Masson's trichrome (Sigma) and imaged using an EVOS XL Core (Invitrogen). For immunohistochemistry staining, slides were rehydrated and exposed to heat mediated antigen retrieval with a sodium citrate buffer. iNOS-stained slides were permeabilized with 0.1% Triton-X100 (Sigma) for 10 min at room temperature. Samples were then incubated in blocking buffer consisting of 10% goat serum and 10 mg mL^{-1} Bovine Serum Albumin (BSA) for 1 hr at room temperature. Slides were incubated with anti-iNOS antibody (Abcam, ab3523) at a concentration of 1:150 overnight at 4°C. CD206-stained slides were incubated with anti-CD206 antibody (Abcam, ab64693) at a concentration of 1:150 overnight at 4°C. Slides were then treated with a secondary goat anti-rabbit antibody conjugated to Alexa fluor 647 (Abcam, ab150083) at a concentration of 1:200 for 1 hr at room temperature. Slides were counterstained with DAPI (Thermo). Large tile scans were taken at 40x using confocal microscopy (Leica Stellaris 5). Positive signal

was quantified in ImageJ after thresholding with RenyiEntropy. The area positive for iNOS or CD206 was normalized to area of DAPI.

Statistical Analysis:

All statistics were calculated using GraphPad Prism 9. Statistical significance was assessed by either one-way ANOVA, two-way ANOVA with Tukey's multiple comparisons test, two-way ANOVA with Sidak's multiple comparisons test, or Student's t-test when appropriate. *p*-values <0.05 were considered statistically significant.

Supplementary Material

Refer to Web version on PubMed Central for supplementary material.

Acknowledgements

References

[1]. Belleghem SMV, Mahadik B, Snodderly KL, Fisher JP, In Biomaterials Science, Elsevier, 2020, pp. 1289–1316.

[2]. Ashammakhi N, Ahadian S, Darabi MA, El Tahchi M, Lee J, Suthiwanich K, Sheikhi A, Dokmeci MR, Oklu R, Khademhosseini A, Adv. Mater 2019, 31, 1804041.

[3]. Lowen JM, Leach JK, Adv. Funct. Mater 2020, 30, 1909089. [PubMed: 33456431]

[4]. Daly AC, Riley L, Segura T, Burdick JA, Nat. Rev. Mater 2020, 5, 20. [PubMed: 34123409]

[5]. Caldwell AS, Aguado BA, Anseth KS, Adv. Funct. Mater 2020, 30, 1907670. [PubMed: 33841061]

[6]. Pfaff BN, Pruett LJ, Cornell NJ, de Rutte J, Di Carlo D, Highley CB, Griffin DR, ACS Biomater. Sci. Eng 2021, 7, 422. [PubMed: 33423459]

[7]. Griffin DR, Weaver WM, Scumpia PO, Di Carlo D, Segura T, Nat. Mater 2015, 14, 737. [PubMed: 26030305]

[8]. Qazi TH, Wu J, Muir VG, Weintraub S, Gullbrand SE, Lee D, Issadore D, Burdick JA, Adv. Mater 2022, 2109194.

[9]. Xin S, Gregory CA, Alge DL, Acta Biomater. 2020, 101, 227. [PubMed: 31711899]

[10]. Feng Q, Li D, Li Q, Cao X, Dong H, Bioact. Mater 2022, 9, 105. [PubMed: 34820559]

[11]. Qazi TH, Burdick JA, Biomater. Biosyst 2021, 1, 100008. [PubMed: 36825161]

[12]. Lutolf MP, Lauer-Fields JL, Schmoekel HG, Metters AT, Weber FE, Fields GB, Hubbell JA, Proc. Natl. Acad. Sci. U.S.A 2003, 100, 5413. [PubMed: 12686696]

[13]. James BP, Sicheng W, Qiang P-H, Marianne Q-J, FEMS Immunol. Med. Microbiol 2005, 45, 159. [PubMed: 16051068]

[14]. de Rutte JM, Koh J, Di Carlo D, Adv. Funct. Mater 2019, 29, 1900071.

[15]. Ji C, Khademhosseini A, Dehghani F, Biomaterials 2011, 32, 9719. [PubMed: 21925727]

[16]. Annabi N, Nichol JW, Zhong X, Ji C, Koshy S, Khademhosseini A, Dehghani F, Tissue Eng., Part B 2010, 16, 371.

[17]. Sideris E, Griffin DR, Ding Y, Li S, Weaver WM, Di Carlo D, Hsiai T, Segura T, ACS Biomater. Sci. Eng 2016, 2, 2034. [PubMed: 33440539]

[18]. Caldwell AS, Campbell GT, Shekiro KMT, Anseth KS, Adv. Healthcare Mater 2017, 6, 1700254.

[19]. Truong NF, Kurt E, Tahmizyan N, Lesher-Pérez SC, Chen M, Darling NJ, Xi W, Segura T, Acta Biomater. 2019, 94, 160. [PubMed: 31154058]

[20]. Xin S, Wyman OM, Alge DL, Adv. Healthcare Mater 2018, 7, 1800160.

[21]. Lv H, Li L, Sun M, Zhang Y, Chen L, Rong Y, Li Y, Stem Cell Res. Ther 2015, 6, 103. [PubMed: 26012510]

[22]. Nih LR, Sideris E, Carmichael ST, Segura T, Adv. Mater 2017, 29, 1606471.

[23]. Mealy JE, Chung JJ, Jeong H, Issadore D, Lee D, Atluri P, Burdick JA, Adv. Mater 2018, 30, 1705912.

[24]. Feng Q, Li Q, Wen H, Chen J, Liang M, Huang H, Lan D, Dong H, Cao X, Adv. Funct. Mater 2019, 29, 1906690.

[25]. Day JR, David A, Kim J, Farkash EA, Cascalho M, Milašinovi N, Shikanov A, Acta Biomater. 2018, 67, 42. [PubMed: 29242160]

[26]. Hao Y, Shih H, Mu oz Z, Kemp A, Lin C-C, Acta Biomater. 2014, 10, 104. [PubMed: 24021231]

[27]. Guimarães CF, Gasperini L, Marques AP, Reis RL, Nat. Rev. Mater 2020, 5, 351.

[28]. Anderson AR, Nicklow E, Segura T, Acta Biomater. 2022, 150, 111. [PubMed: 35917913]

[29]. Hosoyama K, Lazurko C, Muñoz M, McTiernan CD, Alarcon EI, Front. Bioeng. Biotechnol 2019, 7, 205. [PubMed: 31508416]

[30]. Xu T, Random close packing (RCP) on arbitrary distribution of circle sizes.

[31]. Diez-Silva M, Dao M, Han J, Lim C-T, Suresh S, MRS Bull. 2010, 35, 382. [PubMed: 21151848]

[32]. Ginzberg MB, Kafri R, Kirschner M, Science 2015, 348, 1245075. [PubMed: 25977557]

[33]. Murphy KC, Hung BP, Browne-Bourne S, Zhou D, Yeung J, Genetos DC, Leach JK, J. R. Soc., Interface 2017, 14, 20160851. [PubMed: 28179546]

[34]. Fathi-Achachelouei M, Knopf-Marques H, Ribeiro da Silva CE, Barthès J, Bat E, Tezcaner A, Vrana NE, Front. Bioeng. Biotechnol 2019, 7, 113. [PubMed: 31179276]

[35]. Gionet-Gonzales MA, Leach JK, Biomed. Mater 2018, 13, 034109. [PubMed: 29460842]

[36]. Murphy KC, Fang SY, Leach JK, Cell Tissue Res. 2014, 357, 91. [PubMed: 24781147]

[37]. Gonzalez-Fernandez T, Tenorio AJ, Leach JK, 3D Print. Addit. Manuf 2020, 7, 139. [PubMed: 32855996]

[38]. Vorwald CE, Ho SS, Whitehead J, Leach JK, In Biomaterials for Tissue Engineering (Ed.: Chawla K), Springer New York, New York, NY, 2018, pp. 139–149.

[39]. Kouroupis D, Correa D, Front. Bioeng. Biotechnol 2021, 9, 621748. [PubMed: 33644016]

[40]. Koh J, Griffin DR, Archang MM, Feng A, Horn T, Margolis M, Zalazar D, Segura T, Scumpia PO, Carlo D, Small 2019, 15, 1903147.

[41]. Vorwald CE, Joshee S, Leach JK, J. Mol. Med 2020, 98, 425. [PubMed: 32020237]

[42]. Ratner BD, Regener. Biomater 2016, 3, 107.

[43]. Liu Y, Segura T, Front. Bioeng. Biotechnol 2020, 8, 609297. [PubMed: 33363135]

[44]. Pruett LJ, Jenkins CH, Singh NS, Catallo KJ, Griffin DR, Adv. Funct. Mater 2021, 31, 2104337. [PubMed: 34539306]

[45]. Caldwell AS, Rao VV, Golden AC, Bell DJ, Grim JC, Anseth KS, Bioeng. Transl. Med 2021, 6.

[46]. Haschak M, LoPresti S, Stahl E, Dash S, Popovich B, Brown BN, Aging 2021, 13, 16938. [PubMed: 34292877]

[47]. Chen M, Zhang Y, Zhou P, Liu X, Zhao H, Zhou X, Gu Q, Li B, Zhu X, Shi Q, Bioact. Mater 2020, 5, 880. [PubMed: 32637751]

[48]. Sussman EM, Halpin MC, Muster J, Moon RT, Ratner BD, Ann. Biomed. Eng 2014, 42, 1508. [PubMed: 24248559]

[49]. Krzyszczyk P, Schloss R, Palmer A, Berthiaume F, Front. Physiol 2018, 9, 419. [PubMed: 29765329]

[50]. Madden LR, Mortisen DJ, Sussman EM, Dupras SK, Fugate JA, Cuy JL, Hauch KD, Laflamme MA, Murry CE, Ratner BD, Proc. Natl. Acad. Sci. U.S.A 2010, 107, 15211. [PubMed: 20696917]
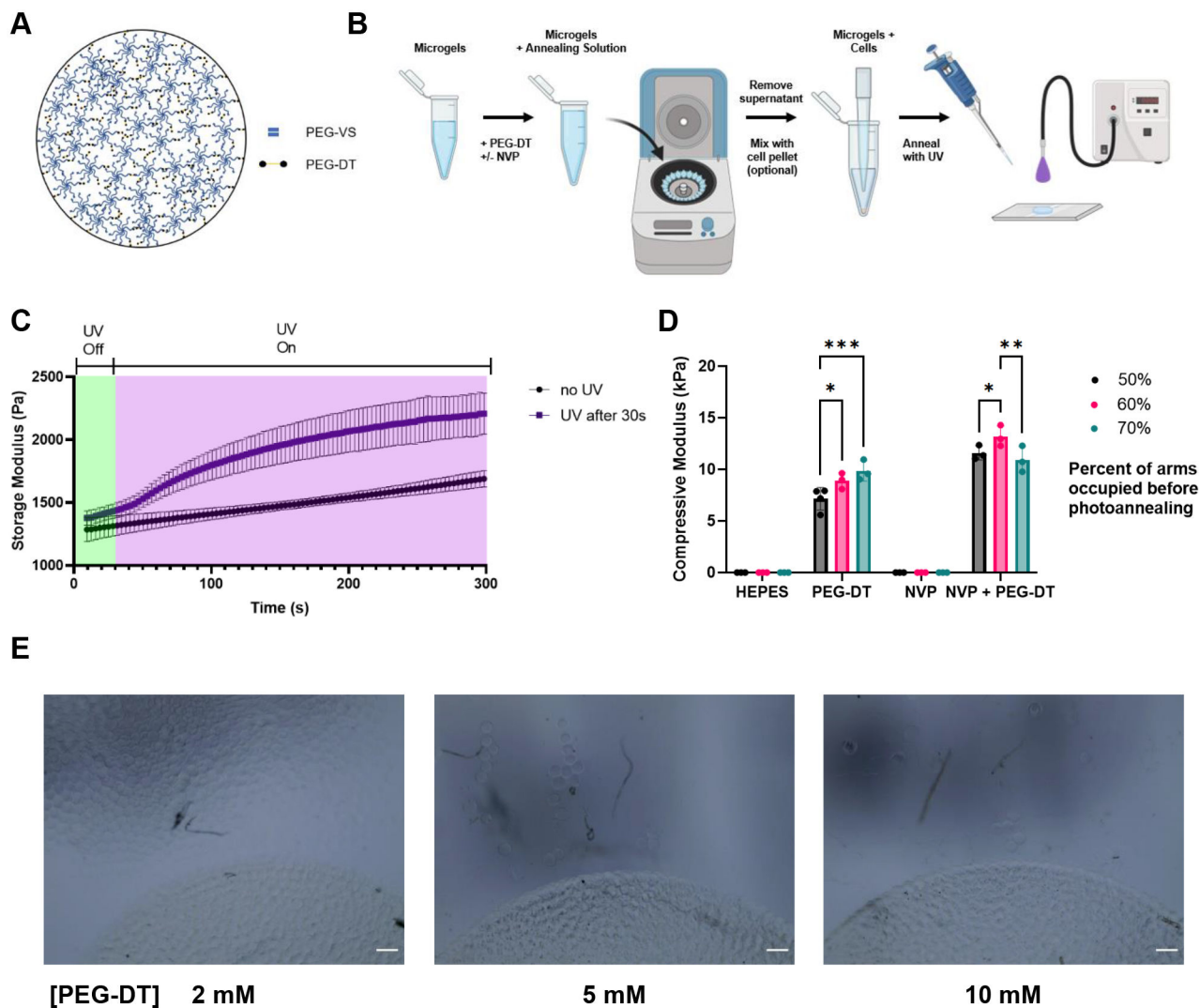
[51]. Whitehead J, Griffin KH, Gionet-Gonzales M, Vorwald CE, Cinque SE, Leach JK, Biomaterials 2021, 269, 120607. [PubMed: 33385687]

[52]. Gonzalez-Fernandez T, Tenorio AJ, Saiz AM Jr, Leach JK, Adv. Healthcare Mater 2022, 11, 2102337.

Figure 1.
Annealing PEG-VS microgels. A) The ratio of PEG-VS to PEG-DT can be stoichiometrically controlled so that arms are left free for annealing. B) Microgels are soaked in an annealing solution containing PEG-DT before being spun down and supernatant aspirated. The microgel slurry is then deposited in the desired location and exposed to UV light for 2 minutes to anneal. C) Storage modulus of microgel scaffolds increases over time when exposed to UV light. D) The annealing solution containing NVP and PEG-DT produced the strongest annealed scaffold. E) A comparison of different PEG-DT concentrations in the annealing solution. A 5 mM solution was sufficient for maximum annealing. Scale bar represents 200 μm. Statistics: two-way ANOVA, Tukey's multiple comparisons test. n   4. *$p < 0.05$, **$p < 0.01$, and ***$p < 0.001$
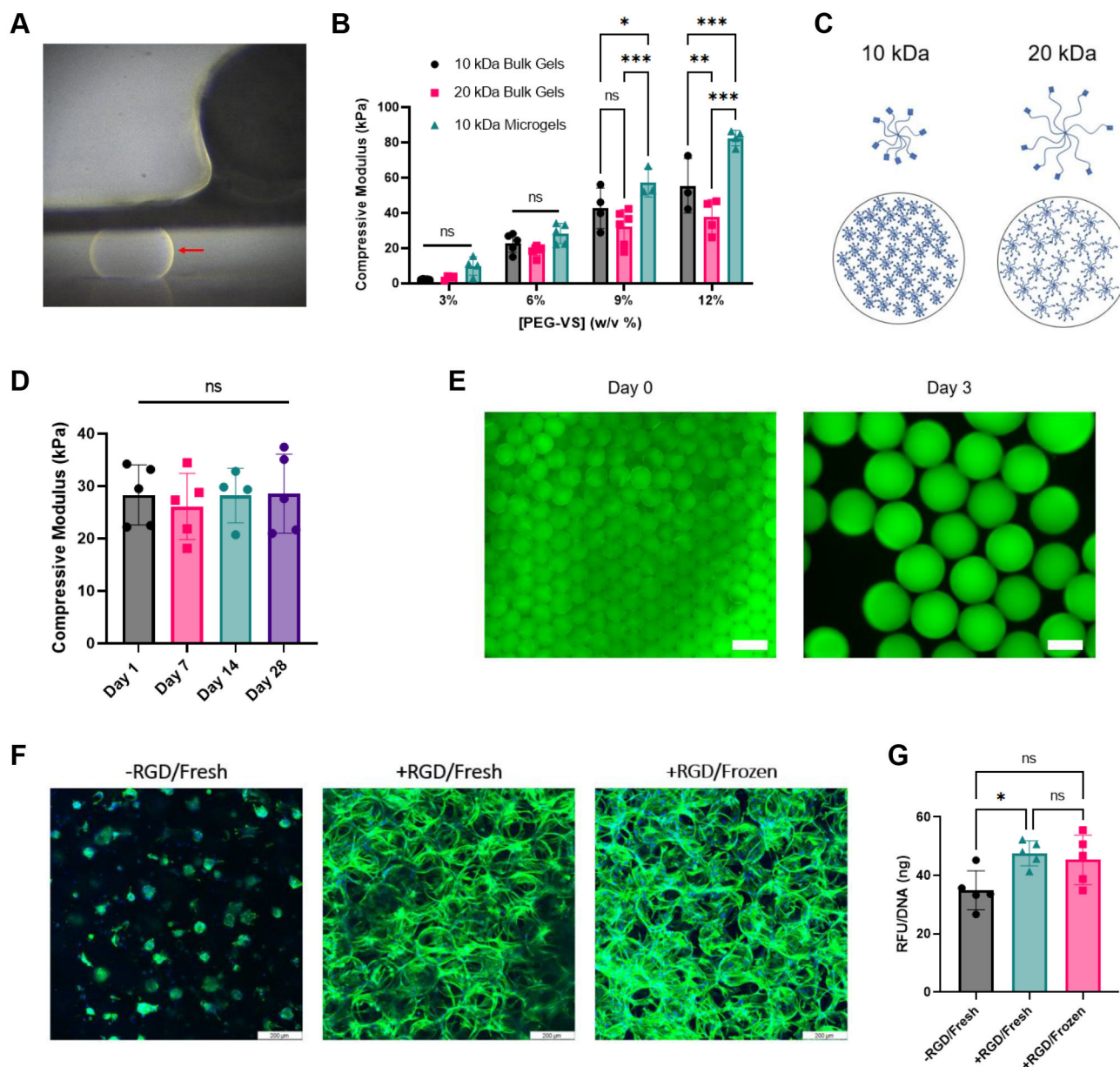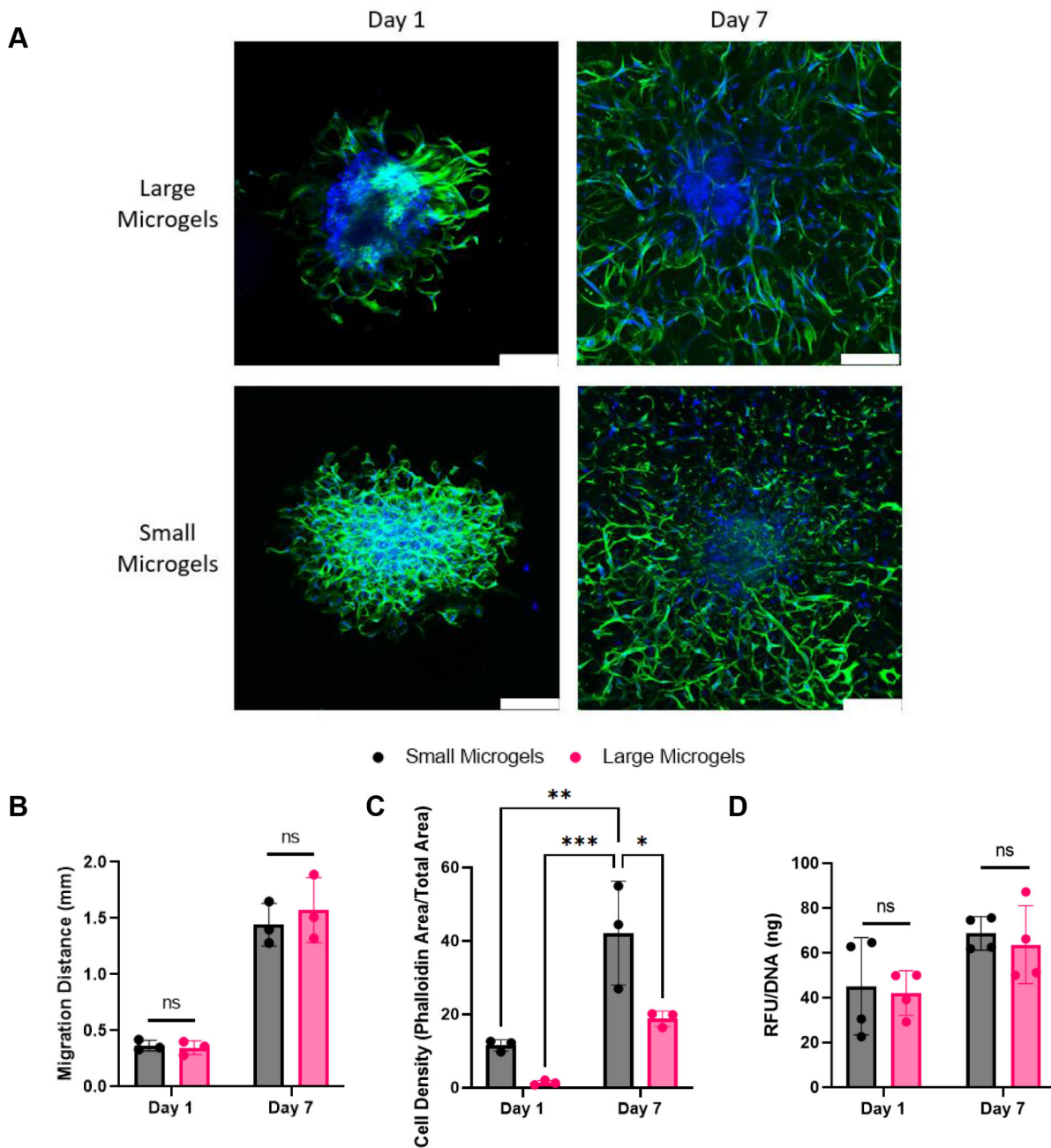
Figure 2.
Mechanical testing and cryopreservation. A) Large microgel (red arrow) compressed between the two plates of the MicroTester. B) Compressive modulus of bulk gels versus microgels. C) 10 kDa PEG-VS monomers pack closer together compared to 20 kDa monomers. D) Compressive modulus of frozen microgels remains constant after thawing. E) Addition of fluorescent peptide to verify successful peptide addition. Scale bar at Day 0 represents 500 μm. Scale bar at Day 3 represents 100 μm. F) Cell spreading on frozen and fresh gels compared to rounded cells on negative control. Scale bar represents 200 μm. G) alamarBlue assay confirms that fresh and frozen microgels support similar levels of bioactivity. Statistics: (B) Two-way ANOVA, Tukey's multiple comparisons test. (D,G) Ordinary one-way ANOVA, Tukey's multiple comparisons test. n ≥ 3. *p < 0.05, **p < 0.01, and ***p < 0.001
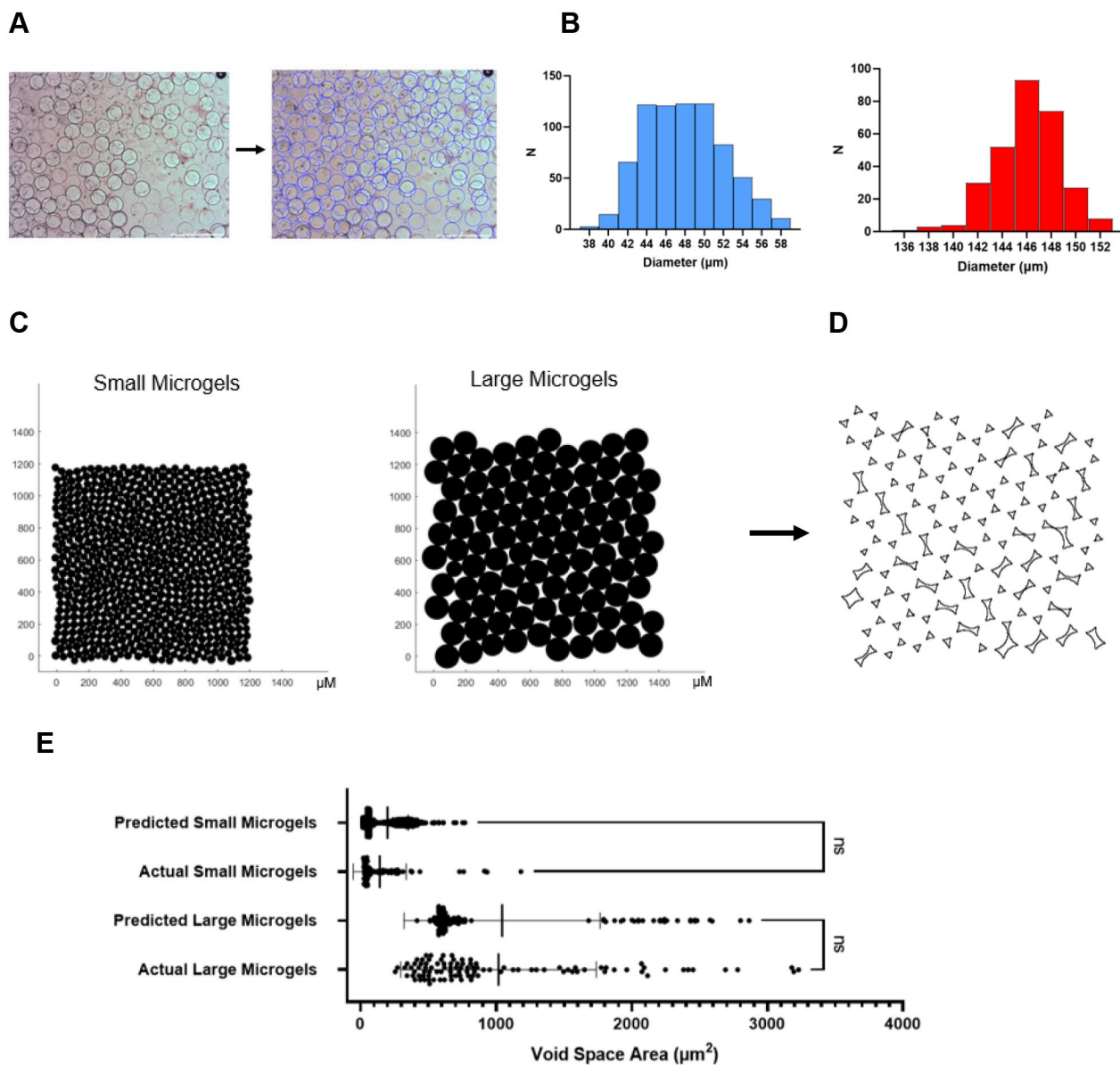
Figure 3.

Modeling void space between microgels in annealed scaffolds. A) Custom MATLAB code detects and measures microgel diameters. Scale bar represents 500 μm. B) Histograms of small and large microgel diameters. C) Modeling microgel annealing in MATLAB. D) Measuring void space area in ImageJ. E) Predicted void space area vs experimentally measured void space area. Statistics: Ordinary one-way ANOVA, Tukey's multiple comparisons test. n ⪆ 100. *$p < 0.05$, **$p < 0.01$, and ***$p < 0.001$
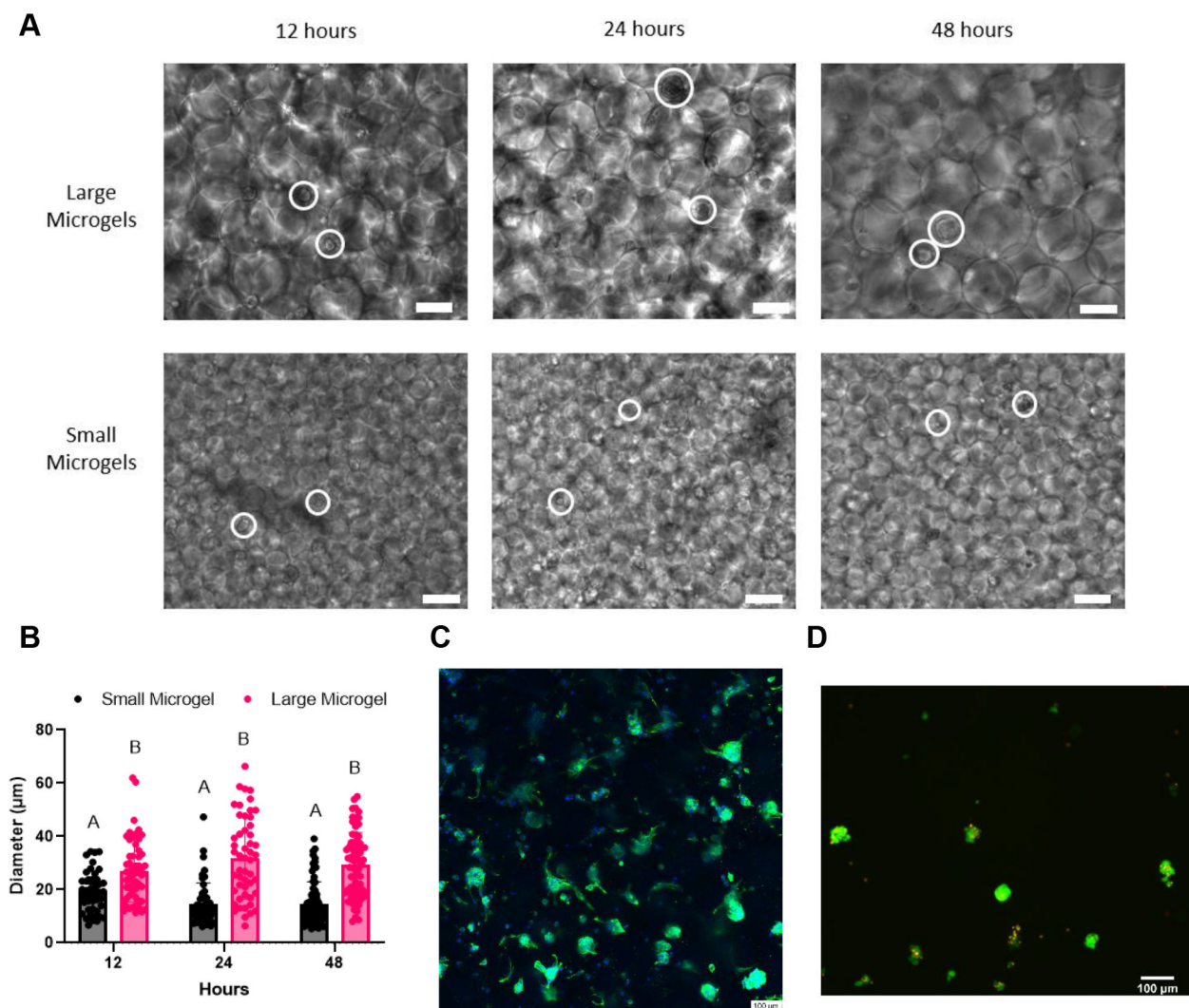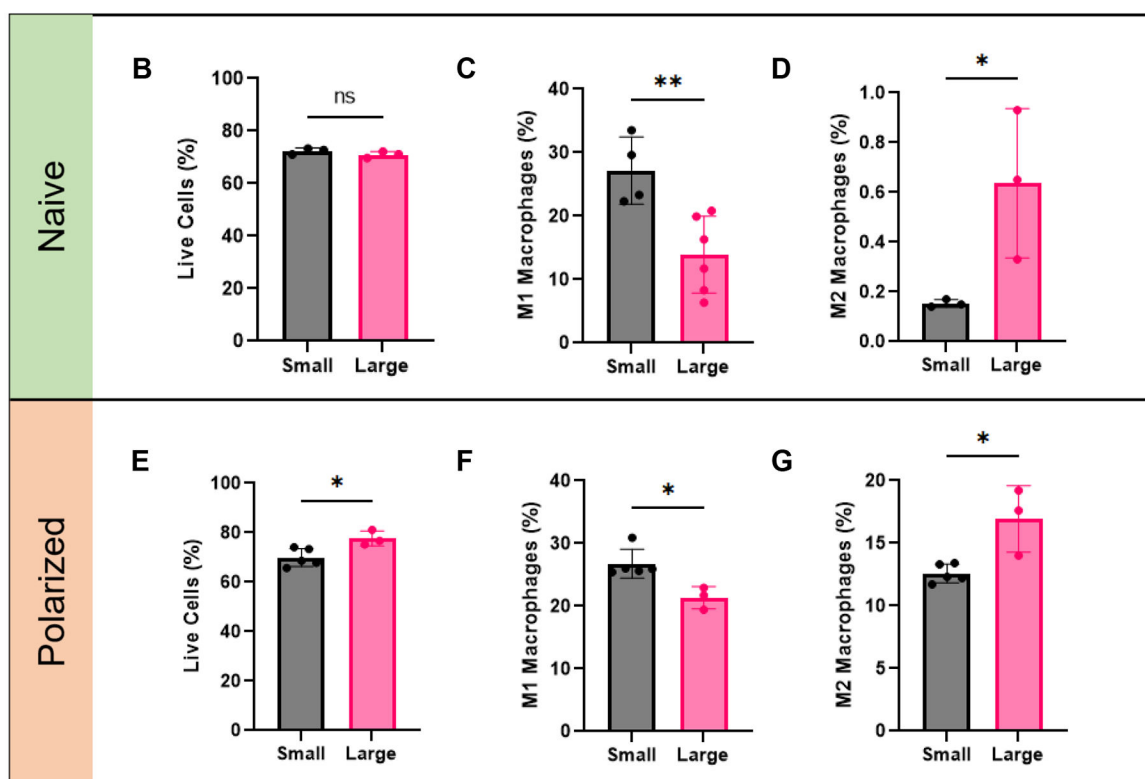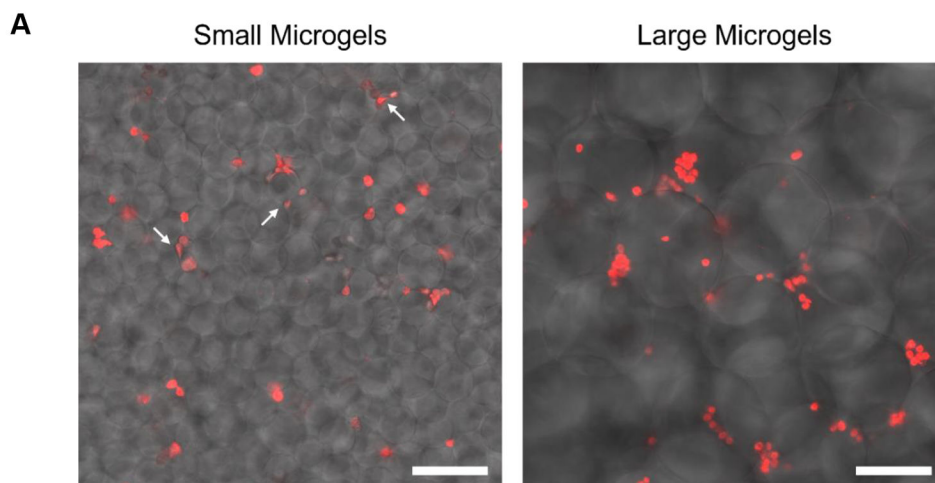
Figure 4.
Microgels as an aggregate-forming platform. A) MSC aggregate formation in large and small microgels over 48 hours. More monodisperse cells are seen in small microgels. MSCs circled in white. B) Quantification of aggregate size demonstrates how larger aggregates form in large microgel scaffolds. C) DAPI/Phalloidin stain reveals the formation of aggregates throughout the large microgel scaffold after 48 hours. D) Live/dead stain of aggregates after retrieval from large microgel scaffolds. Scale bars represent 100 μm. Statistics: two-way ANOVA, Sidak's multiple comparisons test. n   46. $p < 0.05$ was considered significant. Data points with different letters are significantly different from one another.
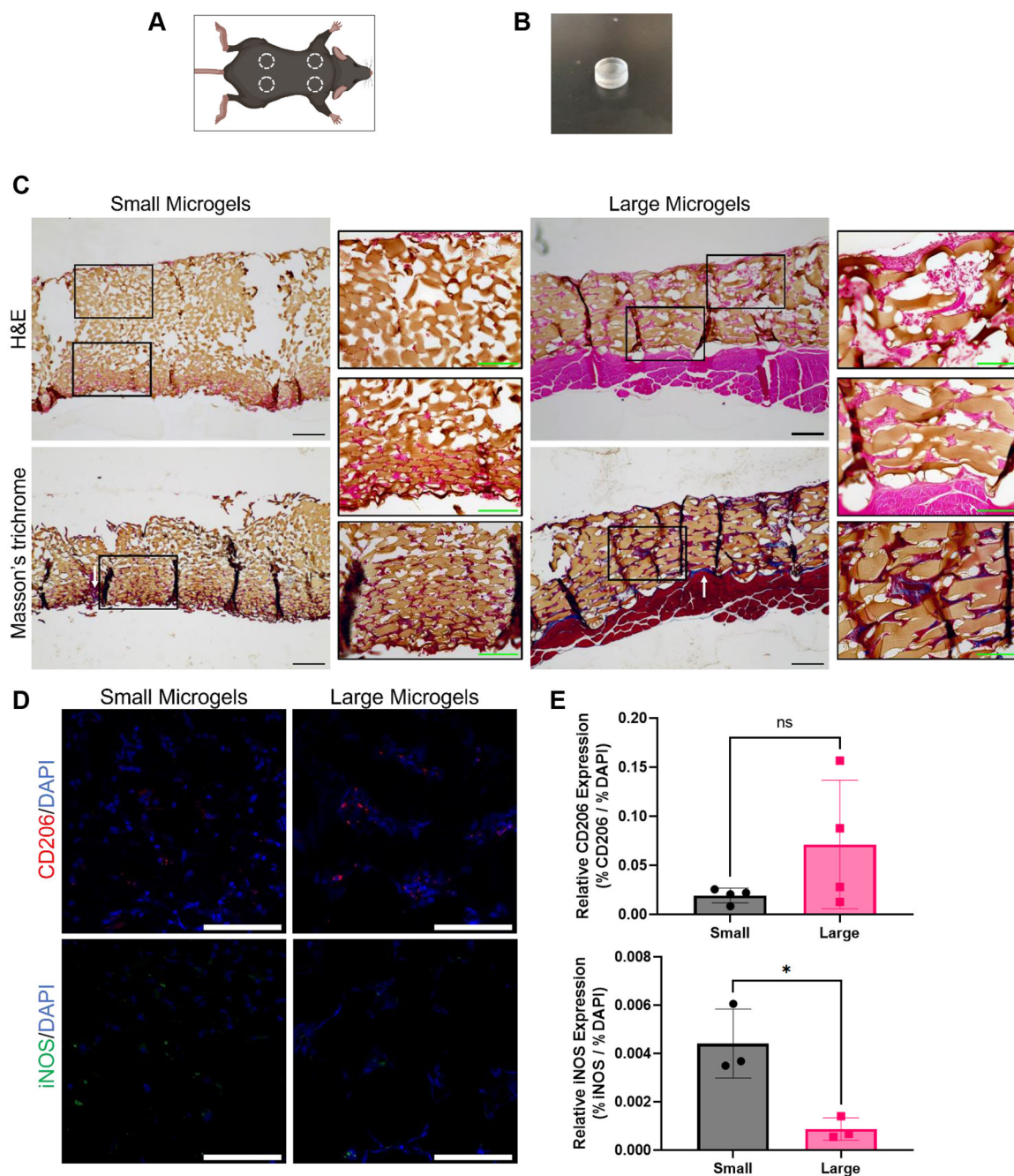
Figure 5.
Spheroids spread rapidly in large and small microgel scaffolds. A) DAPI/Phalloidin stains illustrate that void space inherent in microgel scaffolds facilitates rapid spreading in large and small microgel scaffolds. Scale bars represent 200 μm. B) Migration distance did not differ between microgel scaffolds. C) Cell spreading is denser in small microgel scaffolds versus large microgel scaffolds at Day 1 and Day 7. D) alamarBlue assay confirms that both scaffolds promote high cell metabolic activity. Statistics: Two-way ANOVA, Tukey's multiple comparisons test. n ≥ 3. *p < 0.05, **p < 0.01, and ***p < 0.001

Figure 6.
Microgel size influences macrophage polarization. A) Macrophages (red) in small microgel scaffolds are trapped between them and exhibit an elongated cell morphology (white arrows). Macrophages in large microgel scaffolds are more rounded and can be found in clusters. (B,E) Cell viability is similar in both small and large microgel scaffolds. (C,F) M1 polarization is trending towards being higher in the smaller microgel scaffolds. (D,G) M2 polarization is greater in large microgel scaffolds. Scale bars represent 100 μm. Statistics: Unpaired Student's t tests. n ≥ 4. *p < 0.05, **p < 0.01.

Figure 7.
Subfascial implantation of microgel scaffolds. A) Microgel scaffolds were implanted in four locations per mouse. B) PDMS mold that was loaded with microgels and implanted. C) H&E and Masson's trichrome staining illustrate greater cell infiltration into large microgel scaffolds. Fibrous tissue is sometimes present at the microgel interface (white arrows). Primary scale bars represent 200 μm. Inset scale bars represent 100 μm. D,E) IHC reveals a correlation between microgel diameter and macrophage phenotype. Scale bars represent 100 μm. Statistics: Unpaired Student's t tests. n   3. *p < 0.05.